Observation of an Alfvén Wave Parametric Instability in a Laboratory Plasma

S. Dorfman and T. A. Carter

Phys. Rev. Lett. **116**, 195002 — Published 11 May 2016

DOI: 10.1103/PhysRevLett.116.195002

Observation of an Alfvén wave parametric instability in a laboratory plasma

S. Dorfman and T. A. Carter
University of California Los Angeles, Los Angeles, California 90095, USA

A shear Alfvén wave parametric instability is observed for the first time in the laboratory. When a single finite ω/Ω_i kinetic Alfvén wave (KAW) is launched in the Large Plasma Device above a threshold amplitude, three daughter modes are produced. These daughter modes have frequencies and parallel wave numbers that are consistent with co-propagating KAW sidebands and a low frequency nonresonant mode. The observed process is parametric in nature, with the frequency of the daughter modes varying as a function of pump wave amplitude. The daughter modes are spatially localized on a gradient of the pump wave magnetic field amplitude in the plane perpendicular to the background field, suggesting that perpendicular nonlinear forces (and therefore $k_\perp$ of the pump wave) play an important role in the instability process. Despite this, modulational instability theory with $k_\perp = 0$ has several features in common with the observed nonresonant mode and Alfvén wave sidebands.

PACS numbers: 52.35.Mw, 52.35.Bj

Alfvén waves, a fundamental mode of magnetized plasmas, are ubiquitous in space, astrophysical, and laboratory plasmas. While the linear behavior of these waves has been extensively studied [1–5], nonlinear effects are important in many real systems, including the solar wind and solar corona. Theoretical predictions show that these Alfvén waves may be unstable to various parametric instabilities (e.g. [6–8]) even at very low amplitudes ($\delta B/B < 10^{-3}$). Parametric instabilities could contribute to coronal heating [9], the observed spectrum and cross-helicity of solar wind turbulence [10–12], or damping of fast magnetosonic waves in fusion plasmas [13, 14].

An abundance of theoretical work [6, 7, 15–19] has found three types of parametric instabilities for a $k_\perp = 0$ Alfvén wave: decay, modulational, and beat. The decay instability is the most widely known and involves the decay of a forward propagating Alfvén wave into a backward propagating Alfvén wave and a forward propagating sound wave. By contrast, the modulational instability results in forward propagating upper and lower Alfvénic sidebands as well as well as a nonresonant acoustic mode at the sideband separation frequency. To allow the forward propagating waves to interact, the pump wave must be dispersive – therefore the modulational instability at $k_\perp = 0$ requires finite ω/Ω_i through inclusion of Hall effects [7]. Ponderomotive coupling between the pump and sideband Alfvén modes self-consistently drives the nonresonant density perturbation parallel to the background magnetic field. In this context, "nonresonant" means that the mode does not satisfy a dispersion relation in the absence of the instability drive; this is also called a quasimode in the fusion community [20, 21].

Both shear Alfvén wave decay and modulational instabilities have been produced in numerical simulations [11, 22–25], but observational evidence is limited. Observations in the ion foreshock region upstream of the bow shock in the Earth's magnetosphere have found cases where a decay instability is possible, but results are not conclusive due to limited available data [26, 27].

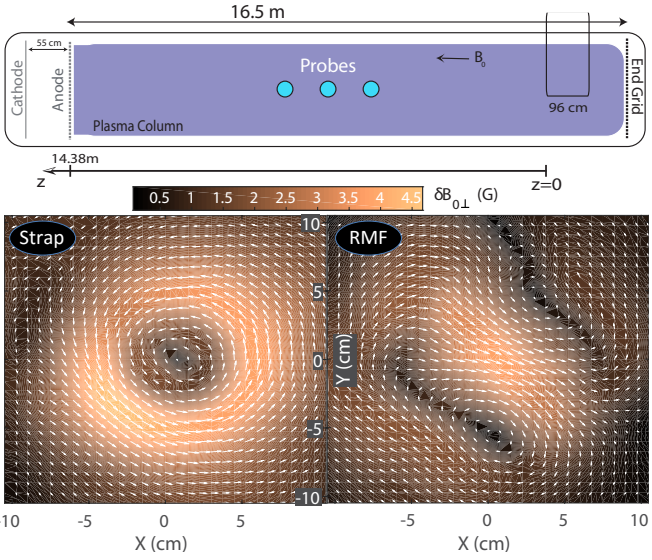

FIG. 1. Experimental setup in LAPD. Top: An Alfvén wave antenna on the right end of the device launches the pump wave. Magnetic and Langmuir probes used to diagnose the interaction are shown. Bottom: Spatial pattern of the pump wave in the xy plane mesured by a magnetic probe at $z = 2.6$ m for the strap antenna (left, $B_0 = 1135$ G) and RMF antenna (right, $B_0 = 993$ G).

In this letter, the first laboratory observations of a shear Alfvén wave parametric instability are presented. A single finite ω/Ω_i, finite $k_\perp$ Alfvén wave is launched, and three daughter waves are observed when the amplitude of the pump is above a threshold: two sideband Alfvén waves co-propagating with the pump and a low frequency nonresonant mode. Frequency and parallel wave number matching relations are satisfied. Although these features of the observed instability are consistent with the $k_\perp = 0$ modulational instability theory, the theoretical growth rate is too small to explain observations.

The spatial pattern of the daughter modes suggests a perpendicular (to the background magnetic field) nonlinear drive.

Experiments are conducted using the Large Plasma Device (LAPD) at UCLA, a cylindrical vessel capable of producing a 16.5 m long, quiescent, magnetized plasma column for wave studies. The BaO cathode discharge lasts for ~ 10 ms, including a several millisecond-long current flattop. Typical plasma parameters for the present study are $n_e \sim 10^{12}$ cm^{-3}, $T_e \sim 5$ eV, and $B_0 \sim 1000$ G ($\beta \sim 10^{-3} - 10^{-4}$) with a fill gas of helium. Extensive prior work has focused on the properties of linear Alfvén waves [5, 28–30]. Studies of the nonlinear properties of Alfvén waves have also been performed on LAPD; in these experiments, two launched Alfvén waves nonlinearly interact to drive: a nonresonant mode [31], a drift wave [32], an acoustic mode [33, 34], or an Alfvén wave [35].

For the present set of experiments, a single antenna is placed at the far end of the LAPD, as shown in the top panel of Fig. 1. This is either the 96 cm long strap antenna [36] shown in the diagram or the rotating magnetic field (RMF) antenna described in Gigliotti et al. [37]. The pump wave is launched at $\omega_0 \sim 0.67\Omega_i$, producing the pattern in the plane perpendicular to B_0 shown for each antenna in the bottom panel. The strap antenna launches a linearly polarized $m = 0$ Alfvén wave cone ($k_{\perp 0}\rho_s = 0.11$) in which oscillating magnetic field vectors (white arrows) circle the field-aligned wave current. By contrast, the RMF antenna is set up to produce two field-aligned current channels ($k_{\perp 0}\rho_s = 0.21$) rotating around B_0 in an $m = 1$ pattern [37]. The rotation direction and hence wave polarization may be controlled by varying the antenna phasing. To ensure the launched wave remains nearly monochromatic, the antenna current is digitized (not shown) and found to contain no significant sideband component.

In the plasma column in front of the antenna, magnetic and Langmuir probes detect the signatures of the pump and daughter modes. Each probe is mounted on an automated positioning system that may be used to construct a 2-D profile in the x-y plane averaged across multiple discharges.

When the pump wave amplitude exceeds a threshold value, additional peaks are observed in the frequency spectrum, as shown in Fig. 2. Panel (A) of the figure shows the appearance of three modes: a low frequency mode (M1), a lower sideband mode (M-), and an upper sideband mode (M+). The frequency matching relations $\omega_\pm \mp \omega_1 = \omega_0$ hold. However, M1 is not purely a density perturbation as predicted by the $k_\perp = 0$ modulational instability theory; as seen in Fig. 2, the mode has significant magnetic character.

A clear parametric dependence of the mode frequencies on pump amplitude is shown in Panel (B) of Fig. 2. As the pump amplitude $\delta B_{0\perp}/B_0$ increases above threshold,

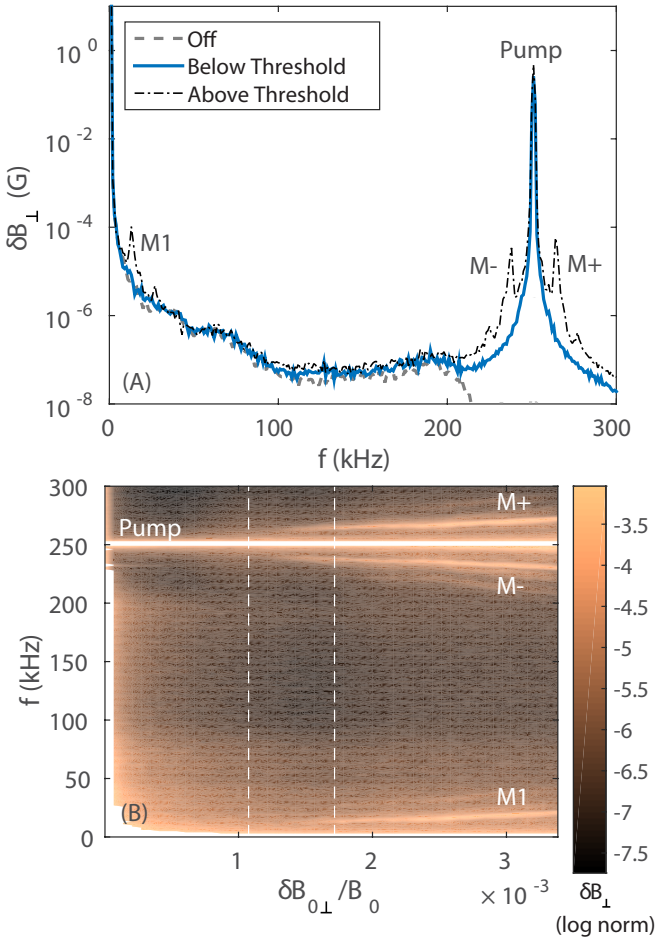

FIG. 2. Observed kinetic Alfvén wave (KAW) parametric instability showing threshold behavior and parametric dependence. RMF antenna, RHCP mode, $B_0 = 993$ G. (A) Frequency spectrum from a magnetic probe at $x = 0$, $y = -6$ cm, $z = 2.6$ m for three pump mode amplitudes. When the pump amplitude is above threshold for instability, three daughter modes are seen. (B) Parametric dependence of the daughter mode frequency as a function of pump amplitude $\delta B_{0\perp}/B_0$. The pump amplitude is 0 on the $\log_{10}$ color scale. White vertical dashed lines represent values of pump amplitude from (A).

the frequencies of M1 and M+ increase; there is a corresponding decrease in the frequency of M- such that frequency matching relations are satisfied at all wave powers.

To determine the character of the three observed daughter modes, the parallel wavenumbers are measured using a set of three axially-separated magnetic probes placed 0.639 m apart, allowing resolution of wave numbers up to $4.9/m$. As shown in Fig. 3, this measurement reveals positive values of $k_\parallel$ for all modes, indicating that all three daughter modes are co-propagating with the pump. Parallel wavenumber matching is satisfied, $k_{\parallel\pm} \mp k_{\parallel 1} = k_{\parallel 0}$. Based on the measured dispersion relation, the pump, M-, and M+ are identified as ki-

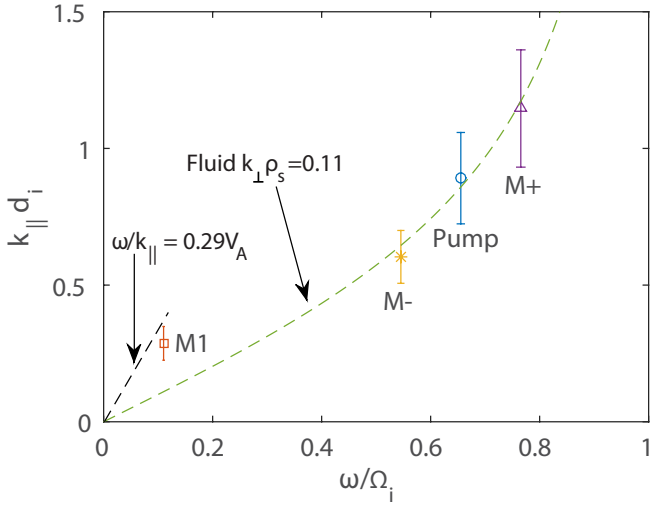

FIG. 3. Parallel wavenumber measurement showing daughter modes co-propagating with the pump. The pump, M-, and M+ are identified as KAWs while M1 is a nonresonant mode. Strap antenna, $B_0 = 1140$ G, $\delta B_{0\perp}/B_0 = 1.9 \times 10^{-3}$. Magnetic probes at $z = 5.11$ m, 5.75 m, and 6.39 m. The fluid dispersion relation for a KAW with the pump $k_{\perp 0}\rho_s = 0.11$ and a line with slope $\omega/k_{||} = 0.29V_A$ are plotted for comparison.

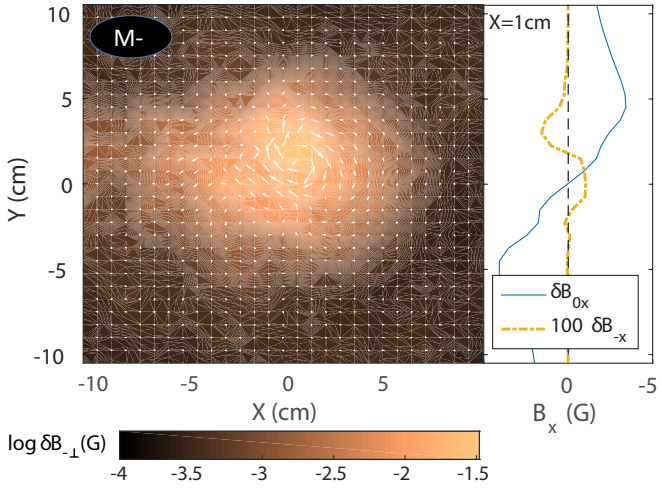

FIG. 4. Spatial profile of M- for the strap antenna suggesting the nonlinearlity is perpendicular in nature. A cut of δB_x is shown on the right. Strap antenna pump from Fig.1, $B_0 = 1135$ G. Color represents fluctuating magnetic field amplitude $\delta B_\perp$; white arrows show realtive magnitude and direction. The peak in M- amplitude occurs on a gradient of the pump mode magnetic field near the current channel center.

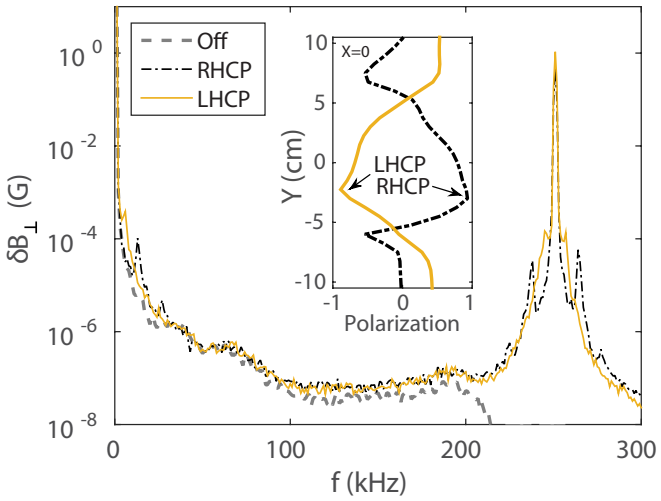

FIG. 5. Dependence of the observed frequecy spectrum on the polarization of the RMF antenna. Mangetic probe $x = 0$, $y = -6$ cm, $z = 2.6$ m. Inset: Polarization of the RMF pump mode from Fig. 1 along a cut at $x = 0$. $B_0 = 993$ G.

netic Alfvén waves (KAWs) while M1 is a nonresonant mode. Note that M1 falls above the KAW dispersion curve $\omega = k_{||}V_A\sqrt{1 + (k_\perp\rho_s)^2 - (\omega/\Omega_i)^2}$ for all possible values of $k_\perp$. However, the measured $k_{||1}$ is too small for M1 to be an acoustic mode (for these parameters, $C_s = 0.012V_A$). This production of a nonresonant mode is consistent with the modulational instability.

Measurements in the plane perpendicular to the background field reveal that perpendicular nonlinear forces likely play a role in generating the observed daughter waves. This is shown in Fig. 4 which displays the pattern of a representative daughter mode M- in the strap antenna case; the plot is derived from a magnetic probe scanned spatially over many shots. By comparing this figure to the strap pump mode pattern in Fig. 1, it can been seen that the amplitude peak of M- occurs near the center of the current channel on a gradient of the pump mode magnetic field. By contrast, the parallel ponderomotive force associated with the modulational instability will produce an amplitude peak in the daughter modes at the location where the pump wave magnetic field peaks [33, 38]. This difference suggests a perpendicular nonlinearity in which perpendicular gradients of the pump mode amplitude (i.e. $k_\perp$) play a key role in the nonlinear terms.

The pump mode polarization also influences the observed instability. This is investigated by changing the RMF antenna phasing to produce one of the two polarization patterns shown in the inset panel of Fig. 5. Polarization is quantified at each spatial point by measuring the ratio of the minor to major radius in the ellipse traced by the rotating magnetic field vector. This quantity is signed negative for left-hand rotation and positive for right-hand rotation. As shown in Fig. 5, left-hand (LHCP) and right-hand (RHCP) pump modes contain opposite polarization mixes that sum to linear polarization. Each mix produces a different frequency spectra in the vicinity of the current channel; the sideband separation frequency produced by LHCP mode is less than half that produced by RHCP mode. As in the linearly polar-

ized strap antenna case, the daughter mode amplitudes peak near the current channel center for RHCP pump mode. The spatial profile and non-linear physics may be different in the LHCP case and is still under investigation; LHCP mode also leads to a broadening of the pump mode profile and a corresponding broad spectrum at low frequencies. The existence of a polarization dependence is consistent with the theoretical literature on parametric instabilities. However, most theoretical work (e.g. [6, 7]) considers uniformly polarized plane waves, making direct comparisons difficult.

Despite important physical differences with the present work, modulational instability theory with $k_\perp = 0$ still describes some features of the observed process well. Fig. 6, Panel (A) shows the roots of the dispersion relation derived by Wong and Goldstein [6], Hollweg [7], solved for LAPD parameters. This two-fluid model outputs the dispersion relation of M1 given a finite amplitude pump wave propagating parallel to the background field. Orange curves for unstable modes reveal the usual decay, beat, and modulational instabilities driven by the parallel ponderomotive force. Because the modulational instability involves only forward propogating modes, it is most consistent with the experimental observations. An arrow on the figure indicates that the peak growth rate of the modulational instability occurs for daughter nonresonant modes with $\omega/k_\parallel = 0.29V_A$. Comparing this value to the measured dispersion of M1 in Fig. 3, the line falls just within the upper errorbar. Therefore, the fact that M1 is not a normal mode of the system is well-predicted by modulational instability theory with $k_\perp = 0$.

The theory also predicts the increase in mode frequency with pump amplitude seen in Fig. 2. This is shown in Panel (B) of Fig. 6 which plots the frequency of M1 for both the experimental case in Fig. 2 (blue circles) and the $k_\perp = 0$ theoretical prediction [6, 7] (red stars). Both theory and experiment follow an upward trend. However, the theoretical frequencies are an order of magnitude too low, and the corresponding growth times are longer than the plasma discharge; clearly, the parallel poderomotive force is too weak to explain the experimental observations. Furthermore, changing the $k_\perp$ spectrum of the pump wave by switching to a different antenna (yellow squares) while keeping other parameters similar results in an increase in the observed M1 frequency. These observations imply that perpendicular structure plays a key role in the observed instability.

Further theoretical development is necessary to fully explain the observed daughter modes. Wong and Goldstein [6], Hollweg [7] predict that the growth rate of the decay instability should be three orders of magnitude larger than that of the modulational instability for the LAPD parameters under investigation. Yet parametric decay to sound waves is not observed. Possible reasons include (1) the growth rates are modified when finite $k_\perp$ is considered and (2) for the larger values of $k_\parallel$ characteristic of the decay instability ion-neutral collisions present in the experiment significantly reduce the growth rate.

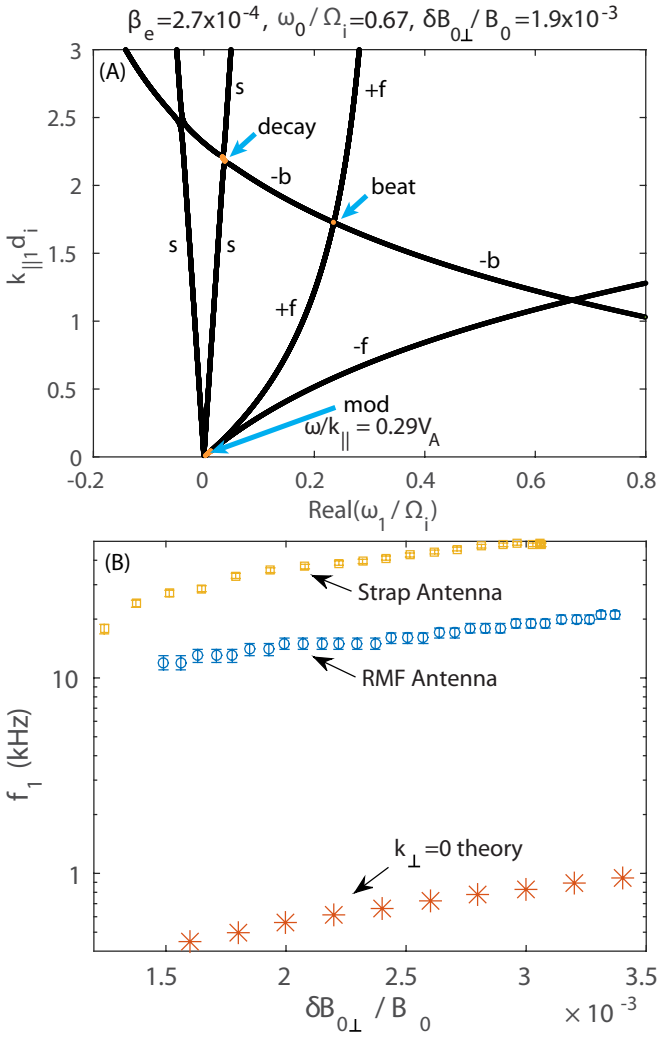

FIG. 6. Comparison between LAPD data and Wong and Goldstein [6], Hollweg [7] $k_\perp = 0$ dispersion relation. (A) Solutions to the dispersion relation of Wong and Goldstein [6], Hollweg [7] for experimental parameters of Fig. 3. Labeled: s: sound mode, -b: backward propagating lower Alfvénic sideband, -f: foward propagating lower Alfvénic sideband, +f: foward propagating upper Alfvénic sideband. Black curves represent stable modes; orange curves repesenting unstable modes are labeled with the appropiate instability. (B) Mode frequency of the modulational instability as a function of pump amplitude for experimental parameters in Fig. 2 (blue circles), theoretical predictions (red stars), and strap antenna results with similar parmeters (yellow squares).

Concerning the effect of finite $k_\perp$, very limited theoretical and computational work is available. Numerical simulations by Del Zanna [39][40], Matteini et al. [23] show a reduction in the growth rate of the decay instability for oblique pump waves, but do not consider the modulational instability. Work by Viñas and Goldstein [41, 42] extend the theory to allow the daughter modes

to have finite $k_\perp$ while retaining $k_{\perp 0} = 0$ for the pump. This allows for new classes of instabilities at oblique angles. In particular, Viñas and Goldstein [42] found a magneto-acoustic instability with a very narrow band of unstable wavenumbers which is favored at low β and high wave dispersion (i.e. high ω/Ω_i). The oblique nature of the daughter modes may also explain the Alfvénic character of the observed nonresonant mode M1. New insight on the nature of the nonlinear terms may also come from extending theoretical work by Brugman [43] which examines co-propagating waves, but only with aligned polarizations. The applicability of these results to the present paper is currently under investigation.

In summary, the first laboratory observations of a shear Alfvén wave parametric instability are presented. A single finite ω/Ω_i, finite $k_\perp$ Alfvén wave is launched above a threshold amplitude, resulting in three daughter modes: two forward propagating Alfvén wave sidebands and a forward propagating nonresonant mode. Frequency and parallel wavenumber matching relations are satisfied. Although these features are consistent with the $k_\perp = 0$ modulational instability theory, the parallel ponderomotive force that drives this process cannot explain the growth or perpendicular spatial profile of the observed daughter modes. Future theoretical and computational work will focus on exploring the role of $k_\perp$ in the instability. Experimental data analysis is ongoing to explore variation with plasma parameters.

The observations reported here open a significant new avenue of research to complement extensive theory [6, 7, 15–19] and simulation [11, 22–25] work on this subject. Features of the observed instability may provide guidance to future space observation aimed at assessing the role of Alfvén wave parametric instabilities in different regions of the heliosphere; for example, in the ion foreshock region of planetary magnetospheres where large amplitude Alfvén waves are generated by ion beams [26, 27, 44]. Because the present results are at low β, they may be of particular interest to the upcoming Solar Probe Plus mission aimed at determining what physical processes are most important in the source region of the solar wind.

The authors thank Y. Lin, R. Sydora, G. Morales and J. Maggs for insightful discussions, S. Vincena, P. Pribyl, S. K. P. Tripathi, and B. Van Compernolle, for insightful discussions and assistance with the experiment, and Z. Lucky, M. Drandell, and T. Ly for their excellent technical support. S. D. was supported by a NASA Jack Eddy Fellowship. This work was performed at the UCLA Basic Plasma Science Facility which is supported by DOE and NSF.

[1] H. Alfvén, Nature **150**, 405 (1942).
[2] J. M. Wilcox, F. I. Boley, and A. W. D. Silva, Physics of Fluids **3**, 15 (1960).
[3] G. J. Morales and J. E. Maggs, Physics of Plasmas **4**, 4118 (1997).
[4] W. Gekelman, J. Geophys. Res **104**, 14417 (1999).
[5] S. Vincena, W. Gekelman, and J. Maggs, Phys. Rev. Lett. **93**, 105003 (2004).
[6] H. K. Wong and M. L. Goldstein, J. Geophys. Res **91**, 5617 (1986).
[7] J. V. Hollweg, J. Geophys. Res **99**, 23431 (1994).
[8] Y. M. Voitenko, Journal of Plasma Physics **60**, 497 (1998).
[9] F. Pruneti and M. Velli, in *Fifth SOHO Workshop: The Corona and Solar Wind Near Minimum Activity*, edited by A. Wilson (1997), vol. 404 of *ESA Special Publication*, p. 623.
[10] B. Inhester, Journal of Geophysical Research: Space Physics **95**, 10525 (1990).
[11] L. D. Zanna, M. Velli, and P. Londrillo, A&A **367**, 705 (2001).
[12] P. H. Yoon and T.-M. Fang, Plasma Physics and Controlled Fusion **50**, 085007 (2008).
[13] J. H. Lee, W. A. Peebles, E. F. Jaeger, E. J. Doyle, N. C. Luhmann, C. C. Petty, R. I. Pinsker, R. Prater, and T. L. Rhodes, Phys. Rev. Lett. **80**, 2330 (1998).
[14] T. Oosako, Y. Takase, A. Ejiri, Y. Nagashima, Y. Adachi, H. Kasahara, T. Yamada, O. Watanabe, H. Tojo, S. Kainaga, et al., Nuclear Fusion **49**, 065020 (2009).
[15] R. Z. Sagdeev and A. Galeev, *Nonlinear plasma theory*, Frontiers in physics (W. A. Benjamin, 1969).
[16] A. Hasegawa and L. Chen, Phys. Rev. Lett. **36**, 1362 (1976).
[17] M. L. Goldstein, ApJ **219**, 700 (1978).
[18] M. Longtin and B. U. . Sonnerup, J. Geophys. Res **91**, 6816 (1986).
[19] J. V. Hollweg, R. Esser, and V. Jayanti, J. Geophys. Res **98**, 3491 (1993).
[20] M. Porkolab, Nuclear Fusion **18**, 367 (1978).
[21] Y. Takase, M. Porkolab, J. J. Schuss, R. L. Watterson, C. L. Fiore, R. E. Slusher, and C. M. Surko, Physics of Fluids **28**, 983 (1985).
[22] S. Ghosh, A. F. Vias, and M. L. Goldstein, Journal of Geophysical Research: Space Physics **98**, 15561 (1993).
[23] L. Matteini, S. Landi, L. Del Zanna, M. Velli, and P. Hellinger, Geophysical Research Letters **37**, n/a (2010).
[24] D. Verscharen, E. Marsch, U. Motschmann, and J. Muller, Phys. Rev. E **86**, 027401 (2012).
[25] X. Gao, Q. Lu, X. Li, L. Shan, and S. Wang, Physics of Plasmas **20**, (2013).
[26] S. R. Spangler, J. A. Leckband, and I. H. Cairns, Physics of Plasmas **4**, 846 (1997).
[27] Y. Narita, K. H. Glassmeier, M. Frnz, Y. Nariyuki, and T. Hada, Nonlinear Processes in Geophysics **14**, 361 (2007).
[28] D. Leneman, W. Gekelman, and J. Maggs, Phys. Rev. Lett. **82**, 2673 (1999).
[29] W. Gekelman, S. Vincena, N. Palmer, P. Pribyl, D. Leneman, C. Mitchell, and J. Maggs, Plasma Physics and Controlled Fusion **42**, B15 (2000).
[30] N. Palmer, W. Gekelman, and S. Vincena, Physics of Plasmas **12**, 072102 (2005).
[31] T. A. Carter, B. Brugman, P. Pribyl, and W. Lybarger, Phys. Rev. Lett. **96**, 155001 (2006).

[32] D. W. Auerbach, T. A. Carter, S. Vincena, and P. Popovich, Phys. Rev. Lett. **105**, 135005 (2010).
[33] S. Dorfman and T. A. Carter, Phys. Rev. Lett. **110**, 195001 (2013).
[34] S. Dorfman and T. A. Carter, Physics of Plasmas **22**, (2015).
[35] G. G. Howes, D. J. Drake, K. D. Nielson, T. A. Carter, C. A. Kletzing, and F. Skiff, Phys. Rev. Lett. **109**, 255001 (2012).
[36] S. T. Vincena, W. A. Farmer, J. E. Maggs, and G. J. Morales, Physics of Plasmas **20** (2013).
[37] A. Gigliotti, W. Gekelman, P. Pribyl, S. Vincena, A. Karavaev, X. Shao, A. S. Sharma, and D. Papadopoulos, Physics of Plasmas (1994-present) **16**, (2009).
[38] G. G. Howes, K. D. Nielson, D. J. Drake, J. W. R. Schroeder, F. Skiff, C. A. Kletzing, and T. A. Carter, Physics of Plasmas **20**, 072304 (2013).
[39] L. Del Zanna, Geophysical Research Letters **28**, 2585 (2001).
[40] L. Del Zanna, L. Matteini, S. Landi, A. Verdini, and M. Velli, Journal of Plasma Physics **81** (2015).
[41] A. F. Viñas and M. L. Goldstein, Journal of Plasma Physics **46**, 107 (1991).
[42] A. F. Viñas and M. L. Goldstein, Journal of Plasma Physics **46**, 129 (1991).
[43] B. T. Brugman, Ph.D. thesis, University of California, Los Angeles (2007).
[44] M. M. Hoppe and C. T. Russell, Journal of Geophysical Research: Space Physics **88**, 2021 (1983).